

# Inclusion of Three-body Correction to Relativistic Equation-of-Motion Coupled Cluster Method: The Application to Electron Detachment Problem

Mrinal Thapa<sup>1</sup> and Achintya Kumar Dutta<sup>1,2</sup>

<sup>1</sup>*Department of Chemistry, Indian Institute of Technology Bombay, Powai, Mumbai 400076, India*

<sup>2</sup>*Department of Inorganic Chemistry, Faculty of Natural Sciences, Comenius University, Ilkovičova 6, Mlynská dolina 84215 Bratislava, Slovakia*

(\*e-mail: [achintya.kumar.dutta@uniba.sk](mailto:achintya.kumar.dutta@uniba.sk))

(\*e-mail: [achintya@chem.iitb.ac.in](mailto:achintya@chem.iitb.ac.in))

(Dated: 26 February 2026)

We present the formulation and implementation of triples correction scheme to the relativistic equation-of-motion coupled-cluster method for ionization potential. Both full and partial triples correction schemes are implemented using the exact two-component atomic mean-field (X2CAMF) Hamiltonian in combination with Cholesky-Decomposition (CD) of two-electron integrals and a frozen natural spinor (FNS) truncation scheme to reduce computational cost. Benchmark calculations on halide anions, noble gas atoms, hydrogen halides, and dihalogen molecules demonstrate that triple excitations are essential for achieving quantitative ionization potentials, reducing mean absolute errors to approximately 0.01–0.08 eV relative to reference and experimental values. The X2CAMF approximation reproduces four-component Dirac–Coulomb results with negligible deviations, while the CD-FNS strategy yields substantial reductions in wall time. The resulting partial triples correction scheme scales as non-iterative  $\mathcal{O}(n^7)$  with storage comparable to CCSD, offering an accurate and practical route for relativistic ionization energy calculations in heavy-element systems.

## I. INTRODUCTION:

Ionization is a fundamental process with far-reaching applications in areas such as spectroscopy, chemical reactivity, and plasma physics. Reliable theoretical models of ionized states are essential for interpreting experimental data. There exists a wide variety of *ab initio* quantum chemistry methods that can theoretically simulate the ionization of atoms and molecules. Among these methods, equation-of-motion coupled-cluster theory (EOM-CC) stands out because of its systematically improvable nature and the capacity to simulate multiple ionized states in a single calculation.<sup>1–3</sup> The EOM-CC method gives identical ionization potential as that of the linear response coupled cluster approach, although the two approaches are derived from very different theoretical perspective.<sup>4–6</sup> An alternative way to calculate ionization energies in the coupled-cluster framework is the  $\Delta$ CC approach, where the ground and ionized states are obtained as the difference of energy obtained from two separate ground-state calculations.<sup>7,8</sup> The EOM-CC approach is advantageous over the  $\Delta$ CC approach, as it can calculate more than one ionized states in a single calculation and also gives access to transition properties. The equation of motion has been extended to relativistic regime<sup>9–13</sup> using two and four component relativistic Hamiltonian. The relativistic IP-EOM-CC is generally used in singles and doubles approximation (IP-EOM-CCSD) and it scales as  $\mathcal{O}(n^6)$  (EOM part scales as  $\mathcal{O}(n^5)$ ). To obtain quantitative accuracy in ionization potential one need to include three-body operators. Musial and co-workers has described the full inclusion of three-body operators in the IP-EOM-CC method.<sup>14</sup> To the best of our knowledge, there has been no report on the inclusion of full triple excitations in relativistic equation-of-motion coupled-cluster methods for ionization potentials. Deprince and co-workers<sup>15</sup> have reported

inclusion of triples in the EOM part over the coupled cluster singles and doubles (CCSD) ground state. The inclusion of triples only the EOM part can improve in the accuracy of the splinting of the ionized states but does not give very accurate IP values. Consequently, most of the high accuracy study on the ionization potential of heavy elements are reported using  $\Delta$ CC approach<sup>16</sup>. Inclusion of partial and full triples correction has been reported for the related (0,1) sector of relativistic fock space multi-reference coupled cluster method<sup>17,18</sup>. The full inclusion of triples to relativistic IP-EOM-CC(IP-EOM-CCSDT) will scales as  $\mathcal{O}(n^8)$ , with ( $\mathcal{O}(n^6)$ ) storage requirement, due to the need for storing ground state triples amplitudes. The computational cost of relativistic IP-EOM-CCSDT will be much higher than the corresponding non-relativistic version, due to lack of spin symmetry, use of uncontracted basis set and need to store complex valued matrix elements.<sup>19,20</sup> Various strategies can be used to reduce the computational cost of relativistic IP-EOM-CCSDT calculations. One can reduce the formal scaling by perturbative truncation of the three-body operator. The floating point operation can be reduced by using truncated natural spinors<sup>21,22</sup>. The efficiency of frozen natural spinors can be further improved by combining them Cholesky-Decomposition (CD) based implementation of two-electron integrals.<sup>11,23</sup> The aim of this manuscript is to develop an efficient triples correction scheme relativistic equation of motion coupled cluster method for ionization potential.

## II. THEORY AND COMPUTATIONAL DETAILS

### A. Relativistic EOM-Coupled-Cluster for Ionised States

One of the most straightforward way to include relativistic effect in quantum chemical calculations is to use a 4-component Dirac-Coulomb Hamiltonian,

$$\hat{H}^{4c} = \sum_i^N \left[ c\vec{\alpha}_i \cdot \vec{p}_i + \beta_i m_0 c^2 + \sum_A^{N_{\text{nuc}}} \hat{V}_{iA} \right] + \sum_{i<j}^N \frac{1}{r_{ij}} \hat{I}_4 \quad (1)$$

Here,  $\alpha$  and  $\beta$  denote the Dirac matrices,  $\sigma$  represents the Pauli spin matrices, and  $\hat{p}$  is the momentum operator. The constants  $c$  and  $m_0$  correspond to the speed of light and the rest mass of the electron, respectively. The operator  $\hat{V}_{iA}$  describes the nuclear potential,  $\hat{I}_4$  is the  $(4 \times 4)$  identity matrix, and  $r_{ij}$  denotes the distance between the  $i^{\text{th}}$  and  $j^{\text{th}}$  electrons.

The above equation for many electron system is solved using the mean-field approximation in the form of Dirac-Hartree-Fock(DHF) method. The DHF wavefunction  $|\Psi_0\rangle$ , is a single determinant made up of 4-component spinors, where the large and small components correspond to the electronic and positronic degrees of freedom, respectively. The correlation calculations are usually done under the no-pair approximation.<sup>24</sup>

The coupled cluster ansatz<sup>1,2,25-27</sup>  $|\Psi_{\text{CC}}\rangle$  based on a DHF wave-function  $|\Psi_0\rangle$  is given as,

$$|\Psi_{\text{CC}}\rangle = e^{\hat{T}} |\Psi_0\rangle \quad (2)$$

The cluster operator  $\hat{T}$  in Eq. (2) can be expressed as follows,

$$\hat{T} = \sum_n \hat{T}_n \quad (3)$$

$\hat{T}_n$  are the set of excitation operators up to  $n^{\text{th}}$  excitation manifolds and can be written in terms of second quantized operators,

$$\hat{T}_n = \sum_{\substack{i<j<k<\dots \\ a<b<c<\dots}} t_{ijk\dots}^{abc\dots} \{ \hat{a}_a^\dagger \hat{a}_b^\dagger \hat{a}_c^\dagger \dots \hat{a}_k \hat{a}_j \hat{a}_i \dots \} \quad (4)$$

Here  $t_{ijk\dots}^{abc\dots}$  represents the cluster amplitudes,  $\hat{a}^\dagger$  and  $\hat{a}$  are the second quantization creation and annihilation operators, with indices (i, j, k ..) denoting occupied spinors, and (a, b, c ..) representing virtual spinors. The cluster amplitudes can be obtained by solving a set of coupled nonlinear equations.

$$\left\langle \Psi_{ijk\dots}^{abc\dots} \left| \hat{H} \right| \Psi_0 \right\rangle = 0 \quad (5)$$

The relativistic ground-state coupled-cluster energy can be obtained as

$$\langle \Psi_0 | \hat{H} | \Psi_0 \rangle = E_{\text{CC}} \quad (6)$$

Here  $\left\langle \Psi_{ijk\dots}^{abc\dots} \right|$  denote different excited-state determinants. The similarity transformed Hamiltonian  $\bar{H}$  is expressed as following,

$$\bar{H} = e^{-\hat{T}} \hat{H}^{4c} e^{\hat{T}} \quad (7)$$

The  $\hat{T}$  operators are generally used in singles and doubles approximation (CCSD)

$$\hat{T} = \hat{T}_1 + \hat{T}_2 \quad (8)$$

It scales iteratively as  $\mathcal{O}(n^6)$  with the size of the basis set. The CCSD method has a storage requirement which scales as  $\mathcal{O}(n^4)$  of the basis set, and it arises due to the need to store the two-electron integrals and coupled-cluster amplitudes. The full inclusion of triples will lead to the CCSDT method

$$\hat{T} = \hat{T}_1 + \hat{T}_2 + \hat{T}_3 \quad (9)$$

It scales iteratively as  $\mathcal{O}(n^8)$  with the size of the basis set, while the storage requirement scales as  $\mathcal{O}(n^6)$ . The primary reason for the increased storage requirement from CCSD to CCSDT is the need to store six-index three-body amplitudes, which can quickly become a computational bottleneck. The coupled-cluster ground-state formalism can be extended to excited states using the equation-of-motion approach. In this approach, the target state wave-function is generated by applying linearized excitation operators to the reference determinant  $|\Psi_{\text{CC}}\rangle$  such that,

$$|\Psi_k\rangle = \hat{R}_k |\Psi_{\text{CC}}\rangle \quad (10)$$

The Hamiltonian operating on this state  $|\Psi_k\rangle$  would give its energy,

$$\hat{H}^{4c} |\Psi_k\rangle = E_k |\Psi_k\rangle \quad (11)$$

For ionized states operator  $\hat{R}_k$  has the form,

$$\hat{R}_k = \sum_i r_i \{ \hat{a}_i \} + \sum_{i<j}^a r_{ij}^a \{ \hat{a}_a^\dagger \hat{a}_j \hat{a}_i \} + \sum_{\substack{i<j<k \\ a<b}} r_{ijk}^{ab} \{ \hat{a}_a^\dagger \hat{a}_b^\dagger \hat{a}_k \hat{a}_j \hat{a}_i \} + \dots \quad (12)$$

The ionization energy can be obtained by solving (9) in its commutator form,

$$[\bar{H}, \hat{R}_k] |\Phi_0\rangle = (E_k - E_0) \hat{R}_k |\Phi_0\rangle = \omega_k \hat{R}_k |\Phi_0\rangle \quad (13)$$

Here,  $\omega_k$  is the ionization energy for the  $k^{\text{th}}$  ionized-state. Since the  $\bar{H}$  is non-Hermitian, it will have both left and right eigen vectors. They are bi-orthogonally related to each other,

$$\langle \Phi_0 | \hat{L}_i \hat{R}_j | \Phi_0 \rangle = \delta_{ij} \quad (14)$$

For ionized states, the  $\hat{L}_k$  operator is defined as,

$$\hat{L}_k = \sum_i l^i \{ \hat{a}_i^\dagger \} + \sum_{i<j}^a l_{ij}^{ij} \{ \hat{a}_i^\dagger \hat{a}_j^\dagger \hat{a}_a \} + \sum_{\substack{i<j<k \\ a<b}} l_{ijk}^{ij} \{ \hat{a}_i^\dagger \hat{a}_j^\dagger \hat{a}_k^\dagger \hat{a}_b \hat{a}_a \} + \dots \quad (15)$$

For the calculation of IP, it is sufficient to solve either Eq. 12 or Eq. 17. However, the calculation of the transition property requires the calculation of both. Equations (12) and (17) are generally solved using Davidson's iterative diagonalization technique<sup>28</sup>. In the IP-EOM-CCSD approximation the Eq. 12 and Eq. 17. are truncated up to the second term. The so-called "sigma" equation construction scales as iteratively  $\mathcal{O}(n^5)$  with the storage requirement similar to the ground

state CCSD method. In the IP-EOM-CCSDT method, the Eq. 12 and Eq. 17. are truncated up to the third term. The EOM diagonalization process scales iteratively as  $\mathcal{O}(n^7)$ , with an additional  $\mathcal{O}(n^5)$  storage requirement for the three-body EOM amplitudes. The programmable expressions for the IP-EOM-CCSDT method have been provided in the supporting information

### 1. Approximate Triples

Most of the computational cost in IP-EOM-CCSDT arises from constructing the six-body  $\hat{T}_3$  term, which scales as  $\mathcal{O}(n^8)$ . Many iterative and non-iterative approximations to non-relativistic EOM-CCSDT are available in the literature.<sup>29-34</sup> In this study, we use the approach introduced by Stanton and co-workers<sup>34</sup>, where the ground state triples amplitudes are approximated at their lowest order.

$$\hat{T}_3^{[2]} = \hat{D}_3^{-1}[\hat{V}, \hat{T}_2] \quad (16)$$

Here  $\hat{D}_3$  are the Møller-Plesset (MP) denominators in triples-triples space i.e.  $(\hat{D}_3)_{ijk}^{abc} = \varepsilon_i + \varepsilon_j + \varepsilon_i - \varepsilon_a - \varepsilon_b - \varepsilon_c$  for semi-canonical Fock operator  $f_j^i = \delta_{ij}\varepsilon_i$ ,  $f_b^a = \delta_{ab}\varepsilon_a$ .  $\hat{T}_3^{[2]}$  is then used to correct the CCSD amplitudes ( $\hat{T}_1$  and  $\hat{T}_2$ ) to the lowest order.

$$\hat{T}_1^\Delta = \hat{D}_1^{-1}[\hat{V}, \hat{T}_3^{[2]}]; \hat{T}_2^\Delta = \hat{D}_2^{-1}[\hat{F} + \hat{V}, \hat{T}_3^{[2]}] \quad (17)$$

Here,  $\hat{D}_1$  and  $\hat{D}_2$  are Møller-Plesset (MP) denominators for the singles-singles and doubles-doubles spaces, respectively, similar to  $\hat{D}_3$ . The corrected singles and doubles amplitudes can be written as follows.

$$\hat{T}_1^{corr} = \hat{T}_1 + \hat{T}_1^\Delta; \hat{T}_2^{corr} = \hat{T}_2 + \hat{T}_2^\Delta \quad (18)$$

Using the corrected single and double amplitudes, one can construct the similarity transformed Hamiltonian  $\tilde{H}_{\text{CCSD(T)(a)}}^0$ . This Hamiltonian can be directly used in the EOM calculations. The detailed derivation of the method can be found in the original non relativistic work by Stanton and co workers.<sup>34</sup> The computational cost of IP-EOM-CCSD(T)(a) consists of four main steps: (i) the iterative CCSD ground-state calculation, scaling as  $\mathcal{O}(n^6)$ ; (ii) generation of the perturbative triple amplitudes,  $\hat{T}_3^{[2]}$ ; (iii) construction of  $\tilde{H}_{\text{CCSD(T)(a)}}$  scaling as  $\mathcal{O}(n^7)$ ; and (iv) the iterative calculation of the IP-EOM, also scaling as  $\mathcal{O}(n^7)$  which is the overall cost. The storage requirement remain same as the original IP-EOM-CCSDT. To further improve the computational efficiency of IP-EOM calculations, a perturbative approximation, analogous to the ground-state CCSD(T)(a) method, can be extended to excited states. In this approach, the triples contribution to the excited state is incorporated perturbatively rather than by solving the full excited-state eigenvalue problem. Instead of constructing the full Hamiltonian  $\tilde{H}_{\text{CCSD(T)(a)}}^0$ , the Hamiltonian  $\tilde{H}_{\text{CCSD}}^{corr}$  is constructed with the corrected T-amplitudes ( $\hat{T}_1^{corr}$  and  $\hat{T}_2^{corr}$ ) and then EOM-CCSD equations are solved. Then the ionization energy is corrected perturbatively through the so-called

"star" correction. The correction of 3-internal intermediate ( $\tilde{H}_{mci}^\Delta$ ) for the EOM-CCSD has to be also separately calculated and added. This approach reduces the overall scaling of IP-EOM calculations to  $\mathcal{O}(n^6)$ . The resulting method is denoted IP-EOM-CCSD(T)(a)\*, with the "star" correction<sup>30,31,34</sup> defined as follows,

$$E_{\text{ex}}^* = \frac{1}{36} \sum_{i,j,k,a,b,c} \frac{[\tilde{L}_3]_{ab}^{ijk} * [\tilde{R}_3]_{ijk}^{ab}}{\varepsilon_i + \varepsilon_j + \varepsilon_k - \varepsilon_a - \varepsilon_b - \varepsilon_c + E_{\text{EOM-CCSD}}^{\text{IP}}[H_{(T)(a)}]}, \quad (19)$$

in which,

$$\begin{aligned} [\tilde{L}_3]_{ab}^{ijk} &= \langle \Psi_0 | (L_1 + L_2) \tilde{H}^{[1]} | \Psi_{ijk}^{ab} \rangle, \\ [\tilde{R}_3]_{ijk}^{ab} &= \langle \Psi_{ijk}^{ab} | (\tilde{H}^{[2]} R_1 + \tilde{H}^{[1]} R_2) | \Psi_0 \rangle \end{aligned} \quad (20)$$

and the  $\varepsilon$ 's are molecular spinors.  $\tilde{H}^{[1]}$  and  $\tilde{H}^{[2]}$  denote the similarity transformed correct to first and second orders in terms of Møller-Plesset perturbation theory. The explicit programmable expressions for IP-EOM-CCSD(T)(a)\* are given in the Appendix. The additional advantage in relativistic IP-EOM-CCSD(T)(a)\* correction is does not require the storage of three-body amplitudes for ground or ionized state, so it has a similar storage as that of the relativistic IP-EOM-CCSD method. One can take a further approximation to IP-EOM-CCSD(T)(a)\* by approximation neglecting the effect of ground state triples in the calculations. This will lead to original IP-EOM-CCSD\* method of Stanton and co-workers.<sup>30,31</sup>

### B. X2CAMF Approximation

One can obtain further computational simplification by going to a two-component picture. The four-component Dirac-Coulomb (DC) Hamiltonian is expressed in terms of second quantized notation, can be represented as,

$$\hat{H}^{4c} = \sum_{pq} h_{pq}^{4c} \hat{a}_p^\dagger \hat{a}_q + \frac{1}{4} \sum_{pqrs} g_{pqrs}^{4c, \text{SF}} \hat{a}_p^\dagger \hat{a}_q^\dagger \hat{a}_s \hat{a}_r + \frac{1}{4} \sum_{pqrs} g_{pqrs}^{4c, \text{SD}} \hat{a}_p^\dagger \hat{a}_q^\dagger \hat{a}_s \hat{a}_r \quad (21)$$

The two-electron part is redefined as the sum of spin-free (SF) and spin-dependent (SD) parts.<sup>35</sup> The spin-dependent component is treated within the atomic mean-field (AMF) approximation, exploiting the localized nature of the spin-orbit interactions.

$$\frac{1}{4} \sum_{pqrs} g_{pqrs}^{4c, \text{SD}} \hat{a}_p^\dagger \hat{a}_q^\dagger \hat{a}_s \hat{a}_r \approx \sum_{pq} g_{pq}^{4c, \text{AMF}} \hat{a}_p^\dagger \hat{a}_q = \sum_{pqIA} n_{iA} g_{pIAqIA}^{4c, \text{SD}} \hat{a}_p^\dagger \hat{a}_q \quad (22)$$

Where  $A$  represents the distinct atoms in the molecule,  $i$  is occupied spinors for atom  $A$ , and  $n_{iA}$  denotes their corresponding occupation numbers. Substituting Eq. (22) in Eq. (21), we get,

$$\hat{H}^{4c} = \sum_{pq} h_{pq}^{4c} \hat{a}_p^\dagger \hat{a}_q + \frac{1}{4} \sum_{pqrs} g_{pqrs}^{4c, \text{SF}} \hat{a}_p^\dagger \hat{a}_q^\dagger \hat{a}_s \hat{a}_r + \sum_{pq} g_{pq}^{4c, \text{AMF}} \hat{a}_p^\dagger \hat{a}_q \quad (23)$$

The four-component Hamiltonian above can be transformed into a two-component picture utilizing the relationship between the coefficients of the large and small component wave functions through the  $X$  matrix and the relationship between the coefficients of the large component and the two-component wave function through the  $R$  matrix.

$$C^S = XC^L \quad (24)$$

$$C^L = RC^{2c} \quad (25)$$

The spin-free contribution of the Coulomb interaction  $g^{4c,SF}$  is reduced to the non-relativistic two-electron integrals  $g^{NR}$  when scalar two-electron picture-change (2e-pc) contributions are neglected. The four-component Hamiltonian, after transformation, becomes the two-component X2CAMF Hamiltonian<sup>36</sup>

$$\hat{H}^{X2CAMF} = \sum_{pq} h_{pq}^{X2C} \hat{a}_p^\dagger \hat{a}_q + \frac{1}{4} \sum_{pqrs} g_{pqrs}^{NR} \hat{a}_p^\dagger \hat{a}_q^\dagger \hat{a}_s \hat{a}_r + \sum_{pq} g_{pq}^{2c,AMF} \hat{a}_p^\dagger \hat{a}_q \quad (26)$$

The above Hamiltonian can be written in terms of an effective one-electron operator and a non-relativistic two-electron operator as:

$$\hat{H}^{X2CAMF} = \sum_{pq} h_{pq}^{X2CAMF} \hat{a}_p^\dagger \hat{a}_q + \frac{1}{4} \sum_{pqrs} g_{pqrs}^{NR} \hat{a}_p^\dagger \hat{a}_q^\dagger \hat{a}_s \hat{a}_r \quad (27)$$

Where  $h^{X2CAMF} = h^{X2C} + g^{2c,AMF}$  is the effective one-electron operator. The main advantage of using the above Hamiltonian is that it completely avoids the construction of the relativistic two-electron integrals.<sup>37–39</sup> In the current work, the two-electron integrals are treated using the Cholesky Decomposition (CD) technique.<sup>40,41</sup>

### C. Cholesky Decomposition

Within the Cholesky decomposition (CD) framework<sup>42</sup>, electron repulsion integrals (ERIs) are approximated in the form

$$\langle \mu\nu | \kappa\lambda \rangle \approx \sum_{P=1}^{n_{CD}} L_{\mu\nu}^P L_{\kappa\lambda}^P, \quad (28)$$

where  $\mu, \nu, \kappa, \lambda$  denote atomic spinor indices,  $L_{\mu\nu}^P$  are the Cholesky vectors, and  $n_{CD}$  is their rank. In the present implementation, an iterative one-step decomposition is employed<sup>23</sup>. At each stage, the largest diagonal element of the ERI matrix is identified, and the procedure is repeated until this element falls below a user-defined threshold ( $\tau$ ). Once constructed, the Cholesky vectors are transformed into the molecular spinor basis as

$$L_{pq}^P = \sum_{\mu\nu} C_{\mu p}^* L_{\mu\nu}^P C_{\nu q}. \quad (29)$$

The molecular-orbital Cholesky vectors provide a compact route to evaluate anti-symmetrized two-electron integrals:

$$\langle pq || rs \rangle = \sum_{P=1}^{n_{CD}} (L_{pr}^P L_{qs}^P - L_{ps}^P L_{qr}^P). \quad (30)$$

In this implementation, integrals with three or four external indices (e.g.,  $\langle ab || ci \rangle$  and  $\langle ab || cd \rangle$ ) are generated on demand rather than constructed or stored explicitly, while all other integrals are built explicitly.

### D. Natural Spinors

Frozen Natural Spinors (FNS) has emerged as an efficient framework to reduce the computational cost of relativistic wave-function based calculations<sup>22,43?,44</sup>. Among the various flavours of FNS available<sup>21,45,46</sup>, the MP2-based natural spinors provide the optimal balance between accuracy and computational cost to describe singly ionized states in the relativistic EOMCC framework<sup>10</sup>. The detailed schematic of the construction of MP2 based frozen natural spinors is given as follows:

1. Construct a 1-body RDM using the X2CAMF MP2 method and separate the virtual-virtual block  $D_{ab}$ .

$$D_{ab} = \frac{1}{2} \sum_{cij} \frac{\langle ac || ij \rangle \langle ij || bc \rangle}{\epsilon_{ij}^{ac} \epsilon_{ij}^{bc}} \quad (31)$$

2. Diagonalize  $D_{ab}$  to obtain the eigenvectors ( $V$ ) as virtual natural spinors, followed by the corresponding eigenvalues ( $\eta$ ) as occupation numbers.

$$D_{ab} V = V \eta \quad (32)$$

3. Transform the virtual-virtual block of the Fock matrix ( $F_{vv}$ ) into the truncated basis of natural spinors ( $F_{vv}^{NS}$ ) by applying a predetermined threshold (cutoff) to the occupation numbers.

$$F_{vv}^{NS} = \tilde{V}^\dagger F_{vv} \tilde{V} \quad (33)$$

4. Diagonalize the  $F_{vv}^{NS}$  block to obtain the semi-canonical virtual natural spinors ( $\tilde{Z}$ ) and their associated orbital energies ( $\epsilon$ ).

$$F_{vv}^{NS} \tilde{Z} = \tilde{Z} \epsilon \quad (34)$$

5. Transform the full canonical space into the semi-canonical space with the help of the transformation matrix ( $U$ ).

$$U = \tilde{V} \tilde{Z} \quad (35)$$

Within the compact active virtual space defined by the FNS scheme, the number of floating-point operations and the memory required for the subsequent correlation calculations is significantly reduced.

## E. Implementation and Computational Details

The methods developed in this work are denoted as FNS-IP-EOM-CCSD\*, FNS-IP-EOM-CCSD(T)(a)\*, and FNS-IP-EOM-CCSD(T)(a). They have been implemented in the development version of our in-house quantum chemistry software, BAGH<sup>47</sup>. The package is primarily written in Python, with performance-critical components optimized in Cython and Fortran. BAGH features interfaces with PySCF<sup>48-50</sup>, GAMESS-US<sup>51</sup>, socutils<sup>52</sup>, and DIRAC<sup>53</sup>. The X2CAMF-HF calculations are carried out using the socutils package through its integration with BAGH. Additionally, the FNS-IP-EOM-CCSDT method has been implemented to facilitate direct comparison with the aforementioned methods.

Fig. 1 provides a schematic representation of the complete computational workflow, detailing the construction of the FNS space and the subsequent evaluation of the electron correlation effects. The figure presents a sequential overview of the algorithmic procedure employed by all methods described above with the respective colour code. The IP-EOM-CCSD(T)(a)\* and IP-EOM-CCSD(T)(a) approaches employ an identical ground-state coupled-cluster treatment and differ only in the formulation of the Hamiltonian transformed by similarity ( $\bar{H}$ ), and subsequent EOM calculations. In contrast, IP-EOM-CCSD(T)(a) and IP-EOM-CCSDT share the same  $\bar{H}$  construction and EOM framework. Finally, EOM-CCSD\* and EOM-CCSD(T)(a)\* utilize identical  $\bar{H}$  and EOM operators but differ in the underlying ground-state correlation treatment. All the calculations in this study were performed using CD-X2AMF Hamiltonian unless specifically mentioned otherwise. The frozen core approximation has been employed for all the calculations in this work.

## III. RESULTS AND DISCUSSION

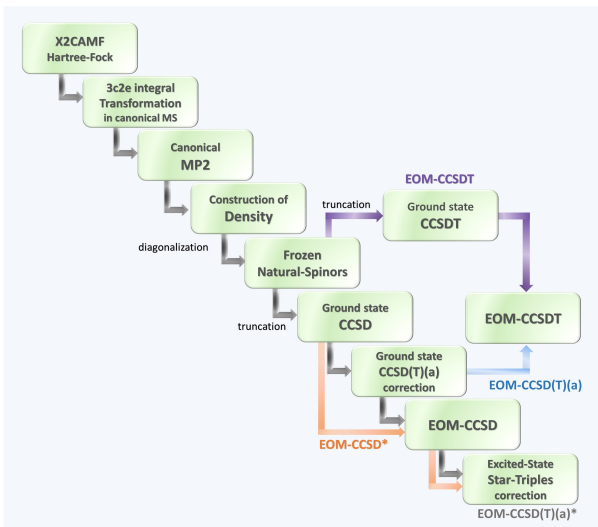


FIG. 1: Schematic representation for different CD-based X2CAMF-FNS methods.

## A. The choice of truncation threshold

The accuracy of FNS based EOM-CCSD depends upon the FNS threshold used for the calculations.<sup>10,21</sup>, also on the CD truncation threshold if CD-X2CAMF approximation is used. Our previous studies<sup>11,23</sup> has shown that the accuracy of the methods are not very sensitive to CD threshold (above a certain limit) and at  $10^{-3}$  gives an optimal balance between computational cost and accuracy. Therefore, we have kept the CD threshold fixed at  $10^{-3}$  in the present study. For the FNS threshold, we have benchmarked it for the HCl molecule using dyall.v3z. Fig. 2 shows the error (with respect to the untruncated canonical virtual space results) vs the FNS truncation threshold for different triples correction scheme for the relativistic IP-EOM-CC method. One can see that all the methods follow same convergence behavior. The IP value for HCl converges at  $10^{-5}$  for all the methods. So, we have chosen this FNS threshold value of  $10^{-5}$  for the subsequent calculations.

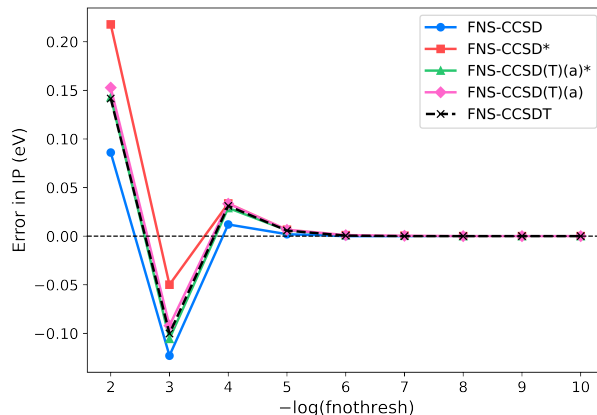


FIG. 2: Convergence of the ionization energy calculated using different EOM-CC methods with respect to the FNS truncation threshold ( $10^{-n}$ ) for the HCl molecule.

## B. The comparison of accuracy in different partial triples correction schemes

To evaluate the accuracy of the methods discussed above, vertical ionization potentials of  $^1S_0$  atoms, including halide ions ( $X^-$ ,  $X = \text{F, Cl, Br, and I}$ ) and noble gases ( $\text{Ne, Ar, Kr, and Xe}$ ), were benchmarked against FNS-IP-EOM-CCSDT calculations performed with the dyall.v3z basis set. The deviations in the energies of the  $^2P_{3/2}$  and  $^2P_{1/2}$  states relative to the reference EOM-CCSDT ionization potentials were systematically analyzed, and the corresponding statistical measures are summarized in Tables S1 and S2 and plotted in Figure 3. Figure 3 shows that EOM-CCSD exhibits a pronounced positive mean error (ME) of approximately 0.06 eV, indicating systematic overestimation of the ionization potentials. In contrast, EOM-CCSD\* yields a negative ME of about  $-0.05$  eV, reflecting systematic underestimation. Both EOM-CCSD(T)(a)\* and EOM-CCSD(T)(a) produce substantially smaller ME values

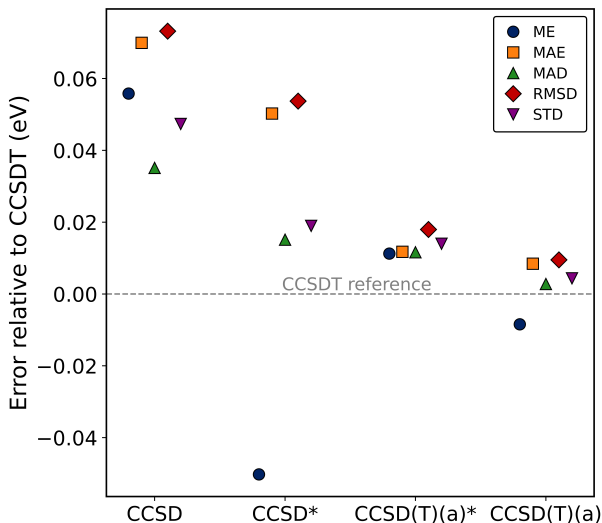


FIG. 3: The deviations in ionization energies of atoms and anions obtained from different IP-EOM-CC methods relative to the reference IP-EOM-CCSDT values. The dyall.v3z basis set was employed for all atoms.

of approximately 0.01 eV and  $-0.01$  eV, respectively, demonstrating much closer agreement with the EOM-CCSDT reference. Notably, methods employing asymmetric treatments of the ground and excited states, such as EOM-CCSD\* and EOM-CCSD(T)(a), tend to underestimate ionization potentials, whereas methods with a more balanced treatment, including EOM-CCSD and EOM-CCSD(T)(a)\*, tend to overestimate them. Similar trends are observed in the mean absolute error (MAE). EOM-CCSD shows the largest MAE (approximately 0.07 eV), followed by EOM-CCSD\* (about 0.05 eV). A significant improvement is obtained with EOM-CCSD(T)(a)\*, for which the MAE decreases to roughly 0.01 eV, while EOM-CCSD(T)(a) yields a comparable value, indicating consistently high accuracy across the dataset. The reduction in error is further reflected in the root-mean-square deviation (RMSD) and standard deviation (STD). EOM-CCSD exhibits the largest dispersion of the errors, with an RMSD of approximately 0.07 eV and an STD of about 0.05 eV. For EOM-CCSD\*, the RMSD is reduced to around 0.05 eV, together with a corresponding decrease in the STD, indicating improved consistency. A further reduction is observed for EOM-CCSD(T)(a)\*, where both RMSD and STD fall in the range of 0.01–0.02 eV. The smallest dispersion is obtained with EOM-CCSD(T)(a), with an RMSD close to 0.01 eV and an STD of approximately 0.004 eV, reflecting tightly clustered errors and minimal residual bias. The maximum absolute deviation (MAD) follows the same overall trend. EOM-CCSD exhibits the largest MAD (about 0.04 eV), which decreases to approximately 0.02 eV for EOM-CCSD\*. For EOM-CCSD(T)(a)\*, the MAD remains well below 0.02 eV and is close to 0.01 eV, while the smallest MAD (about 0.003 eV) is obtained with EOM-CCSD(T)(a). Overall, this analysis demonstrates that IP-EOM-CCSD(T)(a)\* and IP-EOM-CCSD(T)(a) provide efficient and reliable approximations to the full IP-EOM-CCSDT treatment, achieving

substantially reduced systematic and statistical errors across the benchmark set.

### C. Comparison with experimental ionization potentials

For further comparisons, we have calculated the vertical valence ionization potentials of Hydrogen Halides using the partial triples correction scheme developed in this work. The valence dyall basis sets (dyall.vnz;  $n = 2, 3, 4$ ) has been used for the calculation and we have extrapolated them to the CBS limit using the Peterson and Dunning scheme<sup>54</sup>. From Table I, it is evident that both IP-EOM-CCSD(T)(a) and IP-EOM-CCSD(T)(a)\* show good agreement with the experimental results in most cases, with CCSD(T)(a) providing the closest match at the CBS level. In general, all of these methods slightly overestimate the ionization potential compared to experiment, whereas CCSD\* underestimates the IP values in some cases. This trend is almost consistent with that observed for atoms in which we compared the calculated IP with full IP-EOM-CCSDT results. Although the IP-EOM-CCSD(T)(a) method appears to be the most accurate method with least deviation from the experimental value, it is also the most computationally demanding among the four. In contrast, IP-EOM-CCSD(T)(a)\* reproduces comparable results while offering a significant reduction in computational cost. Thus, IP-EOM-CCSD(T)(a)\* provides an optimal balance between computational cost and accuracy, making it an efficient approximation to the full IP-EOM-CCSDT method, and has been used for subsequent calculations in this manuscript.

#### 1. Comparison with 4-component results

The accuracy of the X2CAMF framework for ionization energy calculations at the IP-EOM-CCSD level has been conclusively established in an earlier work from our lab.<sup>11</sup> The present results confirm that this accuracy is preserved upon inclusion of perturbative triple-excitation corrections. Using the FNS-IP-EOM-CCSD(T)(a)\* method, we have evaluated the ionization potentials of halogen hydrides employing three relativistic Hamiltonians: the four-component Dirac–Coulomb Hamiltonian, the spin-free X2C Hamiltonian, and the X2CAMF Hamiltonian. All calculations were performed with the dyall.v4z basis set. The resulting deviations were analyzed through scatter plots. As illustrated in Fig. 4, the X2CAMF Hamiltonian reproduces the four-component Dirac–Hartree–Fock valence ionization potentials with negligible deviations, indicating an accurate treatment of relativistic and spin–orbit effects. In contrast, the spin-free X2C Hamiltonian leads to much larger deviations, highlighting the importance of explicit spin–orbit coupling for reliable ionization energy predictions. The deviation in ionization potentials obtained with the spin-free X2C Hamiltonian is small for lighter systems such as HF and HCl but increases significantly for heavier halogens. This behavior reflects the expected rise in relativistic contributions with increasing nuclear charge, as both scalar and spin-dependent effects scale with the atomic number. In heavier elements,

TABLE I: CBS Ionization potentials (eV) of hydrogen halides in different ionization states computed using coupled-cluster (IP-EOM-CC) methods and compared with experimental values.

Molecule	Ionic State	CCSD	CCSD*	CCSD(T)(a)*	CCSD(T)(a)	Experiment
HF	5 $\Pi$	16.134	16.134	16.217	16.167	16.120 <sup>55</sup>
	4 $\Pi$	16.175	16.173	16.257	16.206	-
	3 $\Sigma$	20.063	20.055	20.138	20.089	19.890 <sup>55</sup>
HCl	9 $\Pi$	12.819	12.691	12.788	12.772	12.744 <sup>56</sup>
	8 $\Pi$	12.902	12.773	12.870	12.854	12.830 <sup>56</sup>
	7 $\Sigma$	16.831	16.696	16.791	16.763	-
HBr	18 $\Pi$	11.739	11.614	11.702	11.694	11.680 <sup>57</sup>
	17 $\Pi$	12.069	11.943	12.030	12.021	11.980 <sup>57</sup>
	16 $\Sigma$	15.837	15.706	15.797	15.776	15.650 <sup>57</sup>
HI	27 $\Pi$	10.440	10.314	10.401	10.397	10.388 <sup>58</sup>
	26 $\Pi$	11.096	10.972	11.058	11.051	11.047 <sup>58</sup>
	25 $\Sigma$	14.470	14.336	14.430	14.405	-
HAt	43 $\Pi$	9.332	9.150	9.263	9.296	-
	42 $\Pi$	11.061	10.876	10.993	11.014	-
	41 $\Sigma$	14.254	14.053	14.177	14.138	-

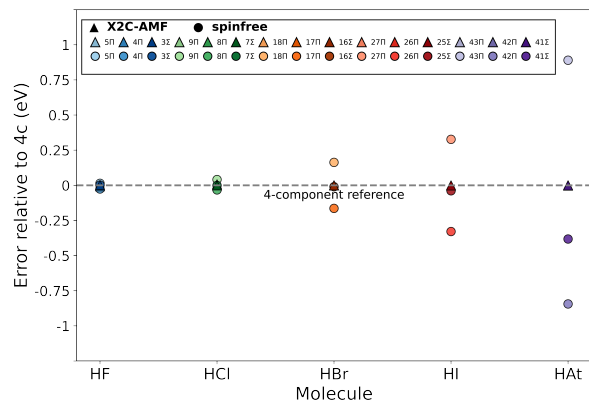


FIG. 4: Deviations in ionization energies computed using X2CAMF and spin-free X2C Hamiltonians relative to the 4-c reference for FNS-IP-EOM-CCSD(T)(a)\*. The basis set dyall.v4z was used for all atoms.

spin-orbit coupling plays an increasingly important role in determining the electronic structure, and its omission in the spin-free X2C formulation leads to noticeable errors in the computed ionization energies. In contrast, the X2CAMF framework incorporates both scalar relativistic and spin-orbit effects, yielding ionization potentials in excellent agreement with the reference 4-c results across the series. Thus, these results indicate that the X2CAMF approach remains a suitable alternative to four-component Hamiltonian for ionization energy calculations beyond the singles-doubles level as well. A key observation is that, for most systems, the first and second ionization potentials (which are of  $\Pi$  type) computed with the spin-free Hamiltonian show comparatively larger deviations, whereas the  $\Sigma$  type third ionization potential exhibits substantially smaller deviations as the inclusion of spin-orbit coupling is not important for that state.

#### D. Ionization of Di-Halogen Molecules

In order to further assess the performance of the FNS-IP-EOM-CCSD(T)(a)\*, we computed the vertical valence ionization potentials of di-halogen molecules ( $X_2$ ;  $X=F, Cl, Br, I$ ) and compared them with CCSD and CCSD\* along with the available experimental data. For  $F_2$  and  $Cl_2$ , uncontracted core-valence Dunning basis sets (aug-cc-pCVNZ,  $N=D, T, Q$ ) were employed, whereas for  $Br_2$  and  $I_2$  core-valence dyall basis sets (dyall.vnz,  $n=2, 3, 4$ ) were used. The resulting ionization potentials were again extrapolated to the complete basis set (CBS) limit using the same Peterson-Dunning scheme<sup>54</sup>. As shown in Table II, all methods generally overestimate the ionization potentials, with only a few exceptions. Among them, CCSD(T)(a)\* provides the most accurate description of the first valence ionization potentials for nearly all di-halogen molecules considered, followed by CCSD and CCSD\*. In almost all cases, the first ionization potentials obtained with CCSD(T)(a)\* lie within the reported experimental uncertainties. In contrast, for the third ionization potentials, CCSD\* exhibits the closest agreement with experiment, followed by CCSD(T)(a)\* and CCSD. Nevertheless, none of the methods is able to reproduce the third ionization potentials within the experimental error bars. The slightly improved performance of CCSD\* relative to CCSD(T)(a)\* for the third ionization potentials can be attributed to fortuitous error cancellation.

The statistical analysis summarized at the bottom of Table II is based on the experimental first and third ionization potentials. All statistical indicators consistently show that CCSD(T)(a)\* provides the most accurate overall description, yielding the smallest ME, MAE, MAD, RMSD, and STD. The near-zero ME indicates the absence of any significant systematic bias, while the low MAE and MAD values reflect a uniformly improved agreement with experimental data across the di-halogen series. In contrast, CCSD exhibits the largest deviations for all statistical measures, indicating a systematic overestimation of the ionization potentials. The CCSD\* approach represents a

TABLE II: CBS ionization potentials (eV) of di-halogen molecules computed using different coupled-cluster methods, compared with experiment.

Molecule	Ionic state	CCSD	CCSD*	CCSD(T)(a)*	Experiment <sup>a</sup>
F <sub>2</sub>	<sup>2</sup> Π <sub>u,3/2</sub>	15.711	15.623	15.773	15.83(0.01)
	<sup>2</sup> Π <sub>u,1/2</sub>	15.756	15.668	15.818	
	<sup>2</sup> Π <sub>g,3/2</sub>	19.051	18.869	19.008	18.80(0.02)
Cl <sub>2</sub>	<sup>2</sup> Π <sub>u,3/2</sub>	11.624	11.451	11.582	11.59(0.01)
	<sup>2</sup> Π <sub>u,1/2</sub>	11.715	11.541	11.673	
	<sup>2</sup> Π <sub>g,3/2</sub>	14.575	14.349	14.467	14.40(0.02)
Br <sub>2</sub>	<sup>2</sup> Π <sub>u,3/2</sub>	10.690	10.452	10.596	10.56(0.01)
	<sup>2</sup> Π <sub>u,1/2</sub>	11.041	10.799	10.945	
	<sup>2</sup> Π <sub>g,3/2</sub>	13.016	12.718	12.856	12.77(0.02)
I <sub>2</sub>	<sup>2</sup> Π <sub>u,3/2</sub>	9.483	9.165	9.351	9.35(0.01)
	<sup>2</sup> Π <sub>u,1/2</sub>	10.120	9.789	9.983	
	<sup>2</sup> Π <sub>g,3/2</sub>	11.362	10.985	11.167	11.01(0.02)
ME		0.150	-0.087	0.061	
MAE		0.180	0.105	0.078	
MAD		0.154	0.080	0.072	
RMSD		0.213	0.122	0.103	
STD		0.152	0.086	0.083	

<sup>a</sup> The experimental values are taken from Ref. <sup>59</sup>.

substantial improvement over CCSD and achieves error magnitudes that are comparable to, albeit slightly larger than, those obtained with CCSD(T)(a)\*. Overall, these results underscore the crucial role of triple-excitation effects in achieving quantitatively reliable ionization potentials for di-halogen molecules. Notably, the significant improvement observed already at the CCSD\* level suggests that perturbative corrections applied at the excited-state level effectively capture the dominant contributions of triple excitations to the ionization potentials of di-halogens.

### E. Time Calculations

To rigorously evaluate the computational performance of the CD-based FNS-IP-EOM-CCSD(T)(a)\* implementation within the X2CAMF framework, a comparative timing analysis was conducted for the HI molecule employing the canonical 4-c, FNS-4-c, and CD based FNS-X2CAMF Hamiltonians. The dyall.v4z basis set was utilized for both hydrogen and iodine atoms, and the frozen-core approximation was applied throughout. The calculations were performed on a dedicated workstation with two Intel(R) Xeon(R) Silver 4210R CPUs @ 2.40 GHz and 512 GB of total RAM. The canonical calculation comprised 18 occupied and 474 virtual spinors. As illustrated in Fig. 5(A), the computational time associated with the IP-EOM-CCSD(T)(a)\* calculation is substantially reduced in the FNS framework relative to the canonical 4-c reference, primarily due to the diminished number of virtual spinors. Within the FNS framework, only 140 virtual spinors are retained. The

canonical calculations required a total wall time of 7 days, 3 hours, 47 minutes, and 15 seconds, whereas the corresponding FNS calculations were completed in 7 hours, 15 minutes, and 51 seconds. Employing the CD-based X2CAMF Hamiltonian further reduces the computational cost dramatically, lowering the total execution time to 1 hour and 55 seconds.

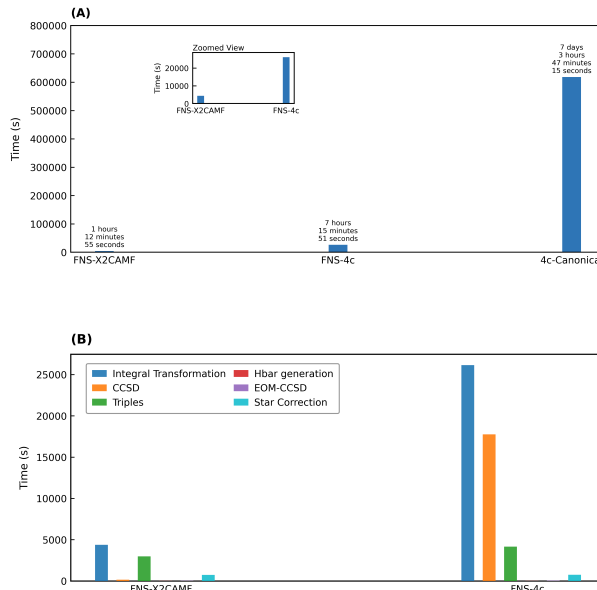


FIG. 5: (A) Comparison of computation times for the evaluation of the correlation energy using the 4c-canonical, 4c-FNS, and CD-X2CAMF-FNS implementations of CCSD(T)(a)\* for the HI molecule. (B) Breakdown of the individual timing components for the 4c-FNS and CD-X2CAMF-FNS implementations. The dyall.v4z basis set was used for both hydrogen and iodine atoms.

Fig. 5(B) presents a more detailed breakdown of the computational timing to compare between the CD-based X2CAMF-FNS-IP-EOM-CCSD(T)(a)\* and 4c-FNS-IP-EOM-CCSD(T)(a)\*. Consistent with our previous studies,<sup>11,23</sup> the substantial reduction in total computational time primarily arises from the significantly high computational cost associated with generating relativistic four-component integrals in the molecular spinor basis. The CD-based X2CAMF approach leads to a substantial reduction in the computational time required for CCSD calculations, consistent with observations reported in earlier studies.<sup>11,23</sup> In contrast, the computational cost associated with the perturbative triples correction is only modestly reduced relative to the corresponding four-component calculations performed within the same FNS space. This limited speedup originates from the fact that some of the terms involved in the ground state triples and excited state triples correction involves 'exchange kind of integrals', the formal scaling of which cannot be reduced using the CD approximation used in the present study. However, the overall cost of the method is still significantly reduced due to the use of FNS and CD-X2CAMF approximation.

## IV. CONCLUSION

We have presented the theoretical formulation, implementation and benchmarking of triples correction to relativistic IP-EOM-CC method. The full IP-EOM-CCSDT and various perturbative approximation to it is tested on a variety of test cases. Among the all the perturbative approximation studied in the work, the IP-EOM-CCSD(T)(a)\* method, which includes the non-iterative triples corrections to both ground and target states, gives the best compromise between computational cost and accuracy and shows significant improvement over relativistic IP-EOM-CCSD method. It circumvents the storage of triples for both ground and target state, thereby substantially reducing the storage requirement while preserving the leading-order effects of triple excitations. The method scales as non-iterative  $O(N^7)$ , with similar storage requirement as that of ground state CCSD method. The floating point operation has been reduced using frozen natural spinors and CD-X2CAMF approximation. An FNS threshold of  $10^{-5}$  gives similar accuracy as that of the untruncated canonical calculation at the fraction of computational costs. The use of CD and X2CAMF approximation gives almost identical result as that of the full component Dirac Coulomb Hamiltonian with significant reduction in computation timing and storage requirement. The newly developed FNS-X2CAMF-IP-EOM-CCSD(T)(a)\* can be routinely applied to atoms and small molecules and will open up door to many interesting applications in physics and chemistry. Work is in progress towards that direction.

## SUPPORTING MATERIAL

The Supporting Material contains the programmable expressions for the relativistic IP-EOM-CCSDT method.

## ACKNOWLEDGMENTS

The authors acknowledge the support from the IIT Bombay, DST-SERB CRG (Project No. CRG/2023/002558), and IIT Bombay supercomputational facility and C-DAC super-computing resources (PARAM Smriti and PARAM Brahma) for computational time. MT acknowledge DST for the inspire fellowship. AKD acknowledges the research fellowship funded by the EU NextGenerationEU through the Recovery and Resilience Plan for Slovakia under project No. 09I03-03-V04-00117.

### Appendix A: Ground State CCSD(T)(a) Triples correction

$$e_i^a = \varepsilon_i - \varepsilon_a. \quad (\text{A1})$$

$$e_{ij}^{ab} = \varepsilon_i + \varepsilon_j - \varepsilon_a - \varepsilon_b. \quad (\text{A2})$$

$$(\hat{D}_3)_{ijk}^{abc} = \varepsilon_i + \varepsilon_j + \varepsilon_k - \varepsilon_a - \varepsilon_b - \varepsilon_c. \quad (\text{A3})$$

$$t_{ijk}^{abc} = \sum_d \langle bc || dk \rangle (\hat{T}_2^{\text{CCSD}})^{ad}_{ij} - \sum_m \langle cm || kj \rangle (\hat{T}_2^{\text{CCSD}})^{ab}_{im}. \quad (\text{A4})$$

$$\hat{T}_3^{|2|} = \frac{\mathcal{P}(i, j, k) \mathcal{P}(a, b, c) t_{ijk}^{abc}}{(\hat{D}_3)_{ijk}^{abc}}. \quad (\text{A5})$$

### 1. T-amplitudes

$$\hat{T}_1^\Delta = \frac{1}{4e_i^a} \sum_{jkbc} \langle jk || bc \rangle (\hat{T}_3^{|2|})_{ijk}^{abc}. \quad (\text{A6})$$

$$\begin{aligned} \hat{T}_2^\Delta = \frac{1}{e_{ij}^{ab}} \left[ \sum_{kc} (\hat{T}_3^{|2|})_{ijk}^{abc} f_k^c \right. \\ \left. + \frac{1}{2} \mathcal{P}(ab) \sum_{kce} (\hat{T}_3^{|2|})_{ijk}^{aec} \langle kb || ce \rangle \right. \\ \left. + \frac{1}{2} \mathcal{P}(ij) \sum_{kic} (\hat{T}_3^{|2|})_{ijk}^{abc} \langle lk || jc \rangle \right]. \end{aligned} \quad (\text{A7})$$

$$\hat{T}_1^{\text{corr}} = \hat{T}_1^{\text{CCSD(T)(a)}} = \hat{T}_1^{\text{CCSD}} + \hat{T}_1^\Delta; \quad (\text{A8})$$

$$\hat{T}_2^{\text{corr}} = \hat{T}_2^{\text{CCSD(T)(a)}} = \hat{T}_2^{\text{CCSD}} + \hat{T}_2^\Delta. \quad (\text{A9})$$

### 2. $\bar{H}$ intermediate

$$\bar{H}_{mcik}^\Delta = \frac{1}{2} \sum_{jkab} t_{ijk}^{abc} \langle mj || ab \rangle. \quad (\text{A10})$$

## Appendix B: Star Triples correction for EOM

### 1. Left-Vector

$$X_1^L = \sum_k \langle ij || ab \rangle l^k \quad (\text{B1})$$

$$X_2^L = \sum_m \langle ji || ma \rangle l_b^{mk} \quad (\text{B2})$$

$$X_3^L = \sum_e \langle ie || ab \rangle l_e^{jk} \quad (\text{B3})$$

$$\tilde{L}_3]_{ab}^{ijk} = \mathcal{P}(i, j, k) [X_1^L - X_2^L] + \mathcal{P}(a, b) X_2^L + \mathcal{P}(i, j, k) X_3^L. \quad (\text{B4})$$

## 2. Right-Vector

$$X_1^R = \sum_{mn} \langle mn || jk \rangle r_n t_{im}^{ab} \quad (\text{B5})$$

$$X_2^R = \sum_e \langle ba || ei \rangle r_{jk}^e \quad (\text{B6})$$

$$X_3^R = \sum_{m,e} \langle mb || ke \rangle r_m t_{ij}^{ae} \quad (\text{B7})$$

$$X_4^R = \sum_{m,b} \langle am || ij \rangle r_{mk}^b \quad (\text{B8})$$

$$[\tilde{R}_3]_{ijk}^{abc} = \mathcal{P}(i, j, k) [X_1^R + X_2^R] - \mathcal{P}(a, b) P(i, j, k) [X_3^R + X_4^R] \quad (\text{B9})$$

### Permutation Notation

$$\mathcal{P}(ij) f(ij) = f(ij) - f(ji), \quad (\text{B10})$$

$$\mathcal{P}(ab) f(ab) = f(ab) - f(ba), \quad (\text{B11})$$

$$\mathcal{P}(ijk) f(ijk) = f(ijk) + f(jki) + f(kij), \quad (\text{B12})$$

$$\mathcal{P}(abc) f(abc) = f(abc) + f(bca) + f(cab). \quad (\text{B13})$$

- <sup>1</sup>J. Čížek, *The Journal of Chemical Physics* **45**, 4256 (1966).  
<sup>2</sup>J. Paldus, J. Čížek, and I. Shavitt, *Phys. Rev. A* **5**, 50 (1972).  
<sup>3</sup>J. F. Stanton and R. J. Bartlett, *The Journal of Chemical Physics* **98**, 7029 (1993).  
<sup>4</sup>D. Mukherjee and P. K. Mukherjee, *Chemical Physics* **39**, 325 (1979).  
<sup>5</sup>H. J. Monkhorst, *International Journal of Quantum Chemistry* **12**, 421 (1977).  
<sup>6</sup>H. Koch and P. Jørgensen, *The Journal of Chemical Physics* **93**, 3333 (1990).  
<sup>7</sup>P. S. Bagus, *Physical Review* **139**, A619 (1965).  
<sup>8</sup>P. S. Bagus and H. F. Schaefer, III, *The Journal of Chemical Physics* **55**, 1474 (1971).  
<sup>9</sup>H. Pathak, S. Sasmal, M. K. Nayak, N. Valal, and S. Pal, *Phys. Rev. A* **90**, 062501 (2014).  
<sup>10</sup>K. Surjuse, S. Chamoli, M. K. Nayak, and A. K. Dutta, *The Journal of Chemical Physics* **157**, 204106 (2022).  
<sup>11</sup>S. Chamoli, M. K. Nayak, and A. K. Dutta, *Journal of Chemical Theory and Computation* **21**, 8823 (2025), pMID: 40947597.  
<sup>12</sup>Y. Wu, Z. Lin, X. Wang, S. Wang, S. H. Southworth, G. Doumy, L. Young, and L. Cheng, *The Journal of Chemical Physics* **163**, 244114 (2025).  
<sup>13</sup>A. Shee, T. Saue, L. Visscher, and A. Severo Pereira Gomes, *The Journal of Chemical Physics* **149**, 174113 (2018).  
<sup>14</sup>M. Musiał, S. A. Kucharski, and R. J. Bartlett, *The Journal of Chemical Physics* **118**, 1128 (2003).  
<sup>15</sup>S. H. Yuwono, R. R. Li, T. Zhang, X. Li, and I. DePrince, A. Eugene, *The Journal of Chemical Physics* **162**, 084110 (2025).  
<sup>16</sup>J. Liu and L. Cheng, *WIREs Computational Molecular Science* **11**, e1536 (2021).  
<sup>17</sup>A. V. Oleynichenko, A. Zaitsevskii, L. V. Skripnikov, and E. Eliav, *Symmetry* **12** (2020).  
<sup>18</sup>A. V. Oleynichenko and A. Zaitsevskii, *The Journal of Chemical Physics* **163**, 224123 (2025).  
<sup>19</sup>M. Reiher and A. Wolf, *Relativistic Quantum Chemistry: The Fundamental Theory of Molecular Science* (John Wiley & Sons, 2015).  
<sup>20</sup>K. G. Dyall and K. Fægri Jr., *Introduction to Relativistic Quantum Chemistry* (Oxford University Press, Oxford, New York, 2007).  
<sup>21</sup>S. Chamoli, K. Surjuse, B. Jangid, M. K. Nayak, and A. K. Dutta, *The Journal of Chemical Physics* **156**, 204120 (2022).  
<sup>22</sup>X. Yuan, L. Visscher, and A. S. P. Gomes, *The Journal of Chemical Physics* **156**, 224108 (2022).  
<sup>23</sup>S. Chamoli, X. Wang, C. Zhang, M. K. Nayak, and A. K. Dutta, *Journal of Chemical Theory and Computation* **21**, 4532 (2025).  
<sup>24</sup>J. Sucher, *Phys. Rev. A* **22**, 348 (1980).  
<sup>25</sup>E. Lindroth, *Phys. Rev. A* **37**, 316 (1988).  
<sup>26</sup>L. Visscher, T. J. Lee, and K. G. Dyall, *The Journal of Chemical Physics* **105**, 8769 (1996).  
<sup>27</sup>L. Visscher, E. Eliav, and U. Kaldor, *The Journal of Chemical Physics* **115**, 9720 (2001).  
<sup>28</sup>K. Hirao and H. Nakatsuji, *Journal of Computational Physics* **45**, 246 (1982).  
<sup>29</sup>J. D. Watts and R. J. Bartlett, *Chemical Physics Letters* **233**, 81 (1995).  
<sup>30</sup>J. F. Stanton and J. Gauss, *Theoretica chimica acta* **93**, 303 (1996).  
<sup>31</sup>J. F. Stanton and J. Gauss, *Theoretica Chimica Acta* **95**, 97 (1997).  
<sup>32</sup>H. Koch, O. Christiansen, P. Jørgensen, A. M. Sanchez de Merás, and T. Helgaker, *The Journal of Chemical Physics* **106**, 1808 (1997).  
<sup>33</sup>K. Kowalski and P. Piecuch, *The Journal of Chemical Physics* **120**, 1715 (2004).  
<sup>34</sup>D. A. Matthews and J. F. Stanton, *The Journal of Chemical Physics* **145**, 124102 (2016).  
<sup>35</sup>K. G. Dyall, *The Journal of Chemical Physics* **100**, 2118 (1994).  
<sup>36</sup>W. Liu and D. Peng, *The Journal of Chemical Physics* **131**, 031104 (2009).  
<sup>37</sup>J. Liu and L. Cheng, *The Journal of Chemical Physics* **148**, 144108 (2018).  
<sup>38</sup>C. Zhang and L. Cheng, *The Journal of Physical Chemistry A* **126**, 4537 (2022), pMID: 35763592.  
<sup>39</sup>S. Knecht, M. Repisky, H. J. A. Jensen, and T. Saue, *The Journal of Chemical Physics* **157**, 114106 (2022).  
<sup>40</sup>T. Uhlřřova, D. Cianchino, T. Nottoli, F. Lipparini, and J. Gauss, *The Journal of Physical Chemistry A* **128**, 8292 (2024).  
<sup>41</sup>C. Zhang, F. Lipparini, S. Stopkowicz, J. Gauss, and L. Cheng, *Journal of Chemical Theory and Computation* **20**, 787 (2024).  
<sup>42</sup>N. H. F. Beebe and J. Linderberg, *International Journal of Quantum Chemistry* **12**, 683 (1977).  
<sup>43</sup>S. Chakraborty, K. Majee, and A. K. Dutta, arXiv preprint arXiv:2511.21640 (2025).  
<sup>44</sup>S. Mandal and A. K. Dutta, *The Journal of Chemical Physics* **164**, 044105 (2026).  
<sup>45</sup>T. Mukhopadhyay, M. Thapa, S. Chamoli, X. Wang, C. Zhang, M. K. Nayak, and A. K. Dutta, *The Journal of Chemical Physics* **163**, 194107 (2025).  
<sup>46</sup>S. Chakraborty, A. Manna, T. D. Crawford, and A. K. Dutta, *The Journal of Chemical Physics* **163**, 044111 (2025).  
<sup>47</sup>A. K. Dutta, A. Manna, B. Jangid, K. Majee, K. Surjuse, M. Mukherjee, M. Thapa, S. Arora, S. Chamoli, S. Haldar, S. Chakraborty, S. Mandal, and T. Mukhopadhyay, "BAGH: A quantum chemistry software package," (2025).  
<sup>48</sup>Q. Sun, *Journal of Computational Chemistry* **36**, 1664 (2015).  
<sup>49</sup>Q. Sun, T. C. Berkelbach, N. S. Blunt, G. H. Booth, S. Guo, Z. Li, J. Liu, J. D. McClain, E. R. Sayfutyarova, S. Sharma, S. Wouters, and G. K.-L. Chan, *WIREs Computational Molecular Science* **8**, e1340 (2018).  
<sup>50</sup>Q. Sun, X. Zhang, S. Banerjee, P. Bao, M. Barbry, N. S. Blunt, N. A. Bogdanov, G. H. Booth, J. Chen, Z.-H. Cui, J. J. Eriksen, Y. Gao, S. Guo, J. Hermann, M. R. Hermes, K. Koh, P. Koval, S. Lehtola, Z. Li, J. Liu, N. Mardirossian, J. D. McClain, M. Motta, B. Mussard, H. Q. Pham, A. Pulkin, W. Purwanto, P. J. Robinson, E. Ronca, E. R. Sayfutyarova, M. Scheurer, H. F. Schurkus, J. E. T. Smith, C. Sun, S.-N. Sun, S. Upadhyay, L. K. Wagner, X. Wang, A. White, J. D. Whitfield, M. J. Williamson, S. Wouters, J. Yang, J. M. Yu, T. Zhu, T. C. Berkelbach, S. Sharma, A. Y. Sokolov, and G. K.-L. Chan, *The Journal of Chemical Physics* **153**, 024109 (2020).  
<sup>51</sup>G. M. J. Barca, C. Bertoni, L. Carrington, D. Datta, N. De Silva, J. E. Deustua, D. G. Fedorov, J. R. Gour, A. O. Gunina, E. Guidez, T. Harville, S. Irle, J. Ivanic, K. Kowalski, S. S. Leang, H. Li, W. Li, J. J. Lutz, I. Magoulas, J. Mato, V. Mironov, H. Nakata, B. Q. Pham, P. Piecuch, D. Poole, S. R. Pruitt, A. P. Rendell, L. B. Roskopf, K. Ruedenberg, T. Sat-

- tasathuchana, M. W. Schmidt, J. Shen, L. Slipchenko, M. Sosonkina, V. Sundriyal, A. Tiwari, J. L. Galvez Vallejo, B. Westheimer, M. Wloch, P. Xu, F. Zahariev, and M. S. Gordon, *The Journal of Chemical Physics* **152**, 154102 (2020).
- <sup>52</sup>X. Wang, “Xubwa/socutils,” (2025).
- <sup>53</sup>T. Saue, L. Visscher, H. J. A. Jensen, R. Bast, A. Severo Pereira Gomes, I. A. Aucar, V. Bakken, J. Brandejs, C. Chibueze, J. Creutzberg, K. G. Dyall, S. Dubillard, U. Ekström, E. Eliav, T. Enevoldsen, E. Fasshauer, T. Fleig, O. Fossgaard, K. J. Gaul, L. Halbert, E. D. Hedegård, T. Helgaker, B. Helmich-Paris, J. Henriksson, M. van Horn, M. Ilias, C. Jacob, S. Knecht, S. Komorovsky, O. Kullie, J. K. Laerdahl, C. V. Larsen, Y. S. Lee, N. H. List, H. S. Nataraj, M. K. Nayak, P. Norman, A. Nyvang, M. Olejniczak, J. Olsen, J. M. H. Olsen, A. Papadopoulos, Y. C. Park, J. K. Pedersen, M. Pernpointner, J. Pototschnig, R. Di Remigio Eikås, M. Repisky, C. M. R. Rocha, K. Ruud, P. Salek, B. Schimmelpfennig, B. SENJEAN, A. Shee, J. Sikkema, A. Sunaga, A. J. Thorvaldsen, J. Thyssen, J. van Stralen, M. López Vidal, s. villaume, O. Visser, T. Winther, S. Yamamoto, and X. Yuan, “Dirac25,” (2025).
- <sup>54</sup>K. A. Peterson, D. E. Woon, and J. Dunning, Thom H., *The Journal of Chemical Physics* **100**, 7410 (1994).
- <sup>55</sup>M. S. Banna and D. A. Shirley, *The Journal of Chemical Physics* **63**, 4759 (1975).
- <sup>56</sup>A. Yench, A. Cormack, R. Donovan, A. Hopkirk, and G. King, *Chemical Physics* **238**, 109 (1998).
- <sup>57</sup>M. Adam, M. Keane, A. Naves de Brito, N. Correia, P. Baltzer, B. Wannberg, L. Karlsson, and S. Svensson, *Journal of Electron Spectroscopy and Related Phenomena* **58**, 185 (1992).
- <sup>58</sup>A. Cormack, A. Yench, R. Donovan, K. Lawley, A. Hopkirk, and G. King, *Chemical Physics* **221**, 175 (1997).
- <sup>59</sup>A. Potts and W. Price, *Transactions of the Faraday Society* **67**, 1242 (1971).